Electronic Supplementary Material (ESI) for Physical Chemistry Chemical Physics.

Supplementary Information for

Tuning Phase Compositions of MoS_2 Nanomaterials for Enhanced Heavy Metal Removal: Performance and Mechanism

Qi Han[a,#], Hao Cao[b,#], Yuchen Sun[a], Gang Wang[c], Sidney Poon[d], Monong Wang[d], Bei Liu[a], Yanggang Wang[b], Zhongying Wang[a*], Baoxia Mi[d]

[a] Department of Environmental Science and Engineering, Southern University of Science and Technology, Shenzhen 518055, China

[b] Department of Chemistry and Guangdong Provincial Key Laboratory of Catalytic Chemistry, Southern University of Science and Technology, Shenzhen 518055, China

[c] Department of Physics, Southern University of Science and Technology, Shenzhen 518055, China

[d] Department of Civil and Environmental Engineering, University of California, Berkeley, California 94720, United States

[*] to whom correspondence should be addressed. e-mail: wangzy6@sustech.edu.cn; tel.: +86-075588018040;

Table of Content

Text 1. Synthesis of MoS_2 with different S/Mo precursor atomic ratio

For the synthesis of MoS_2 using S/Mo precursor atomic ratios of 1:1, 3:1, 5:1, 10:1, a certain amount of thioacetamide and ammonium heptamolybdate tetrahydrate were dissolved in 24 mL deionized water. The mixture was stirred in a magnetic stirring apparatus for 1h, and the mixed solution was then transferred to a 50 mL Teflon-lined stainless-steel autoclave and heated at 180 °C, 200 ℃, 220 ℃ or 240 ℃ for 12 h. After the reaction, the system was terminated by natural cooling to room temperature. The as-synthesized MoS_2 was collected in a centrifuge tube and washed with deionized water and ethanol several times by repeatedly centrifuging, decanting the liquid, and resuspending the solids. The purified samples were stored in DI water in an N_2-filled glove-box. The addition of thioacetamide and ammonium heptamolybdate tetrahydrate was listed in Table S1.

Table S1 Synthesis of MoS_2 with different S/Mo precursor atomic ratio

S/Mo	**1:1**	**2:1**	**3:1**	**5:1**	**10:1**
Thioacetamide/mmol	8.60	17.17	20.23	20.23	20.23
Ammonium heptamolybdate tetrahydrate/mmol	1.23	1.23	0.96	0.58	0.29

Table S2. Pb^{2+} removal performance by other common adsorbent materials.

Adsorbent	**Max capacity**	**Removal mechanism**	**Reference**
Hydrothermal MoS_2	632.91 mg/g (1T) and 81.63 mg/g (2H)	Electrostatic adsorption and S-Pb complexation	this work
δ-MnO_2	10.2 mg/g	Electrostatic adsorption	1
AC/nZVI	59.35 mg/g	Electrostatic adsorption	2
Amio-Fe_3O_4	40.10 mg/g	Electrostatic adsorption	3
Polyaniline grafted chitosan	16.07 mg/g	Electrostatic Adsorption	4
XC-72 carbon	125.0 mg/g	Adsorption and precipitation	5
Fe_3O_4@TMU-32	1600 mg/g	Electrostatic adsorption	6
Magnetic GO	385.1 mg/g	Electrostatic adsorption	7
Thiol-modified biochar	55.4 mg/g	S-Pb complexation	8

Table S3. Pb^{2+} removal performance by MoS_2 nanosheets and composites.

Adsorbent	Max capacity	Removal mechanism	Reference
Hydrothermal MoS_2	632.91 mg/g (1T) and 81.63 mg/g (2H)	Electrostatic adsorption and S-Pb complexation	this work
Chemical exfoliated MoS_2	~740 mg/g	S-Pb complexation, membrane separation	9
Calcined MoS_2	~147.09 mg/g and 64.16 mg/g	S-Pb complexation	10
Hollow MoS_2	~1267 mg/g	S-Pb complexation	11
Hydrothermal MoS_2	26.0 mg/g and 152.0 mg/g	S-Pb complexation	12
MoS_2-N-H	303.04 mg/g	Pb-S complexation and electrostatic adsorption	13
Hydrothermal MoS_2	~293 mg/g	Electrostatic adsorption	14
ferrite-MoS_2-carbon	588.24 mg/g for MnFMC and 660.67 for CoFMC	Inner-sphere complexation and ion-exchange	15
rGO@MoS_2	498 mg/g	Surface complexation	16
MoS_2@biochar	189 mg/g	Metal-sulfur chemical complexation	17
MoS_2@Fe_3O_4	240.7 mg/g	Surface complexation	18
Fe_3O_4@polydopamine -MoS_2	508.9 mg/g	Ion exchange and surface complexation	19
MoS_2/clinoptilolite	50 mg/g	Surface complexation	20
MoS_2/Fe_3O_4	263.6 mg/g	Metal-sulfur chemical complexation	21

Table S4. The comparison of E_{ads} between vacuum model and implicit solvation model.

Model	E_{ads} (vacuum), eV	E_{ads} (vaspsol), eV
MoS_2-Ag (1T)	-4.52	-6.72
MoS_2-Pb (1T)	-6.12	-9.47
MoS_2-Ag (2H)	-0.90	-1.00
MoS_2-Pb (2H)	-1.34	-1.69

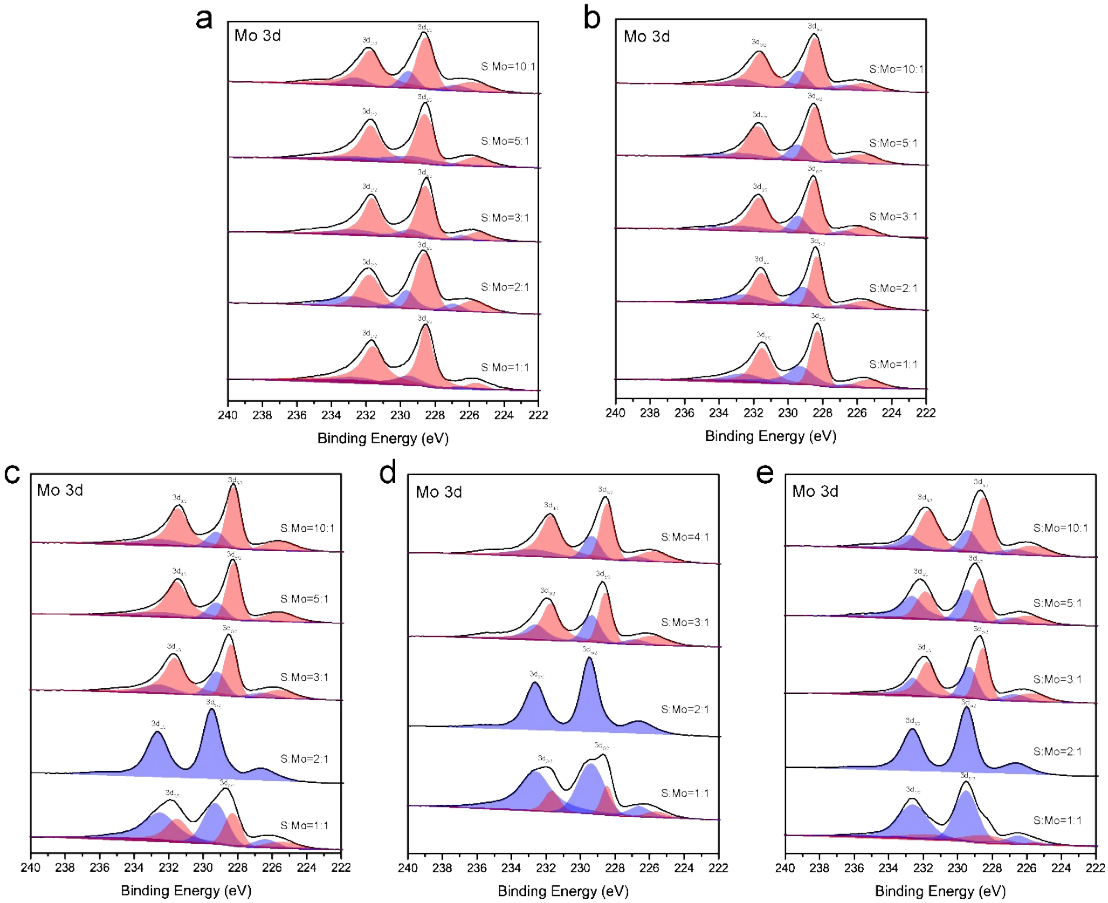

Figure S1. Mo 3d XPS spectra of as-synthesized MoS_2 samples at S/Mo precursor atomic ratios from 1 to 10 and synthesis temperatures of 180℃ (a), 200℃ (b), 220℃ (c), 230℃ (d), and 240℃ (e).

Figure S2. 1T-MoS_2 (left) and 2H-MoS_2 (right) aqueous suspensions.

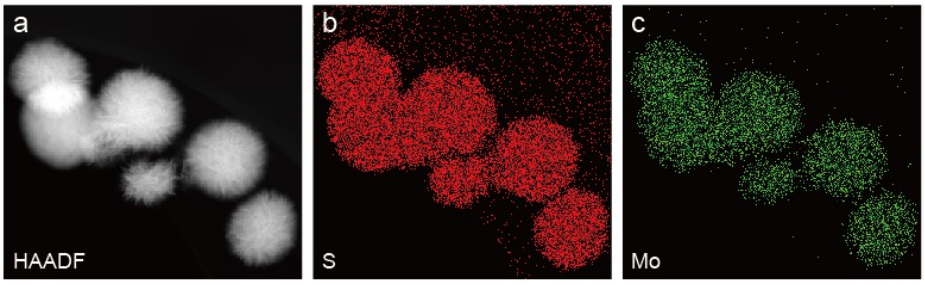

Figure S3. HAADF image of 2H-MoS_2 (a), EDS mapping of S (b) and Mo (c).

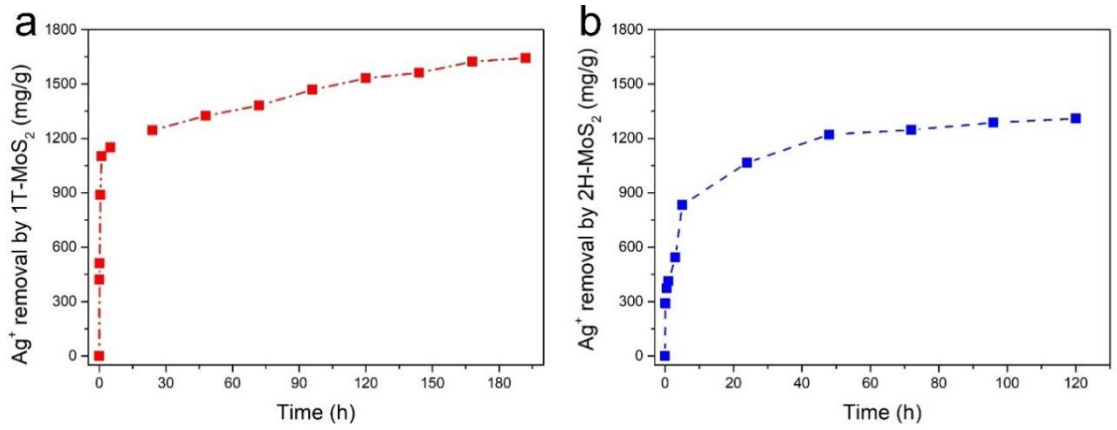

Figure S4. Ag^{+} removals by 1T- (a) and 2H-MoS_2 (b) as a function of reaction time.

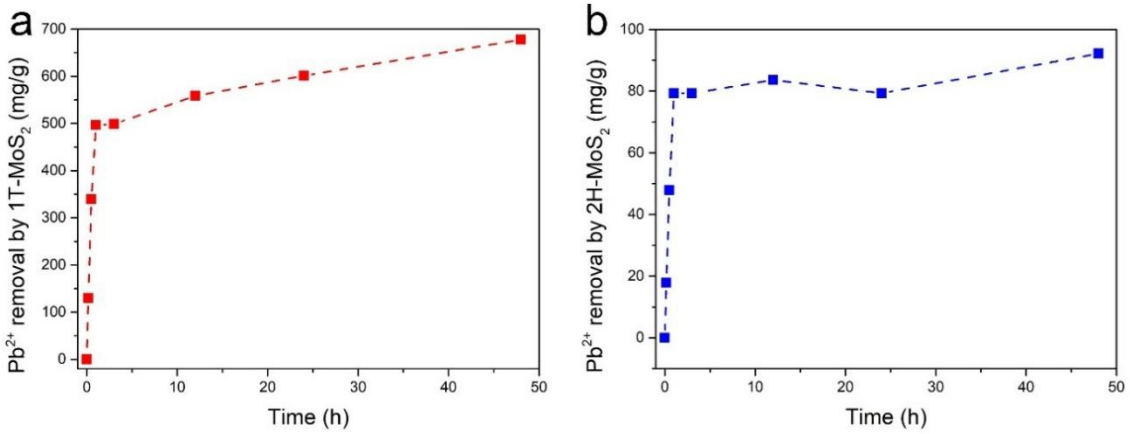

Figure S5. Pb^{2+} removals by 1T- (a) and 2H-MoS_2 (b) as a function of reaction time.

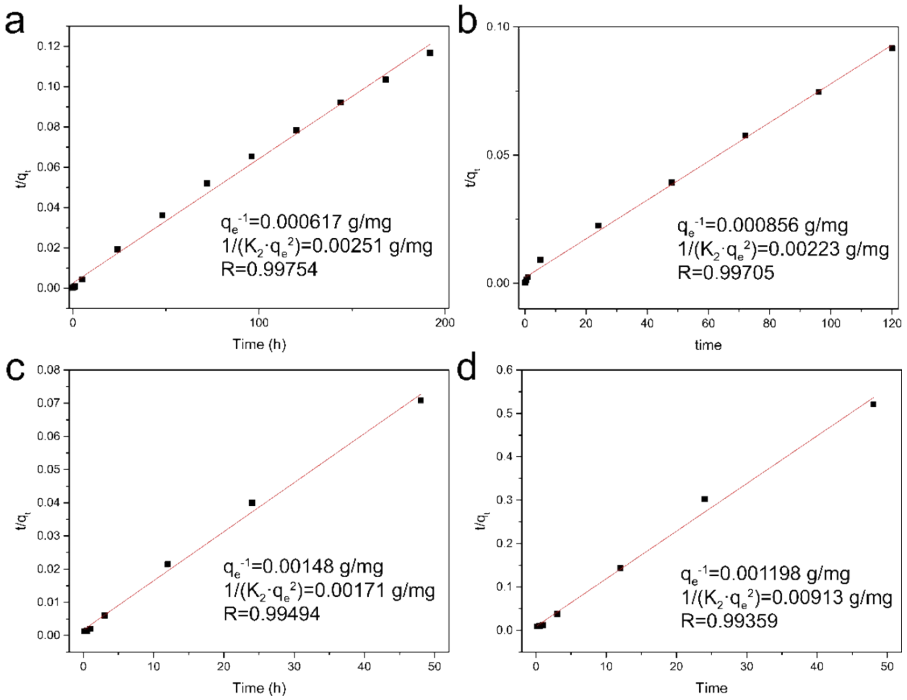

Figure S6. Second-order fitting for the heavy metal ions removal kinetics by using the linear-form formula $\frac{t}{q_t} = \frac{1}{K_2 q_e^2} + \frac{t}{q_e}$. Removal kinetics of (a) Ag^+ by 1T-MoS_2; (b) Ag^+ by 2H-MoS_2; (c) Pb^{2+} by 1T-MoS_2 and (d) Pb^{2+} by 2H-MoS_2.

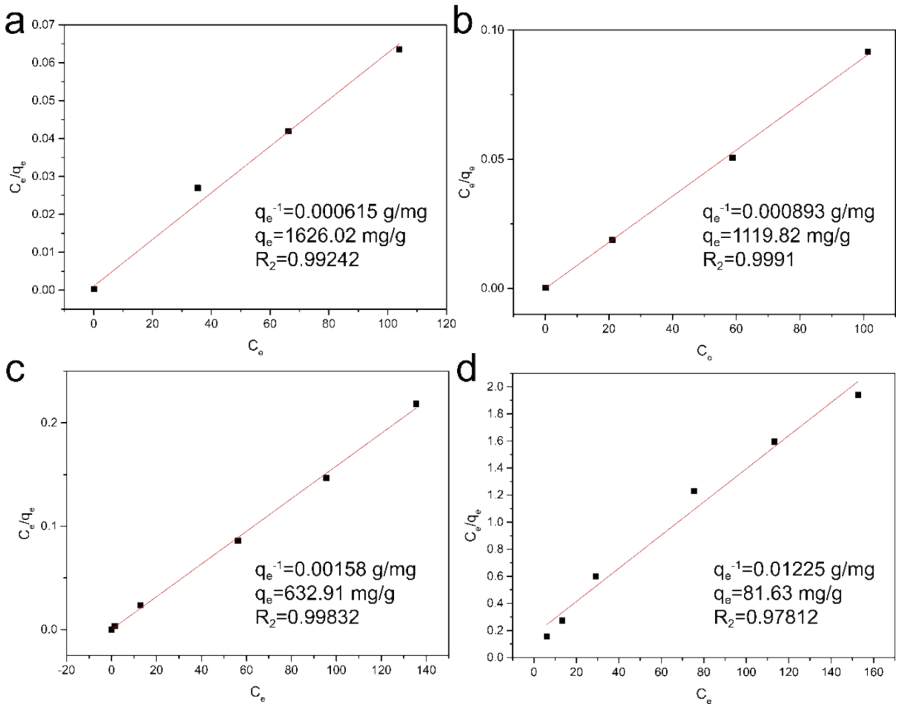

Figure S7. Langmuir fitting of adsorption curves of the heavy metal ions by MoS_2 in Fig. 3. Linear form of Langmuir isothermal model was $\frac{C_e}{q_e} = \frac{1}{q_0 K_L} + \frac{1}{q_0} C_e$ (C_e was equilibrium concentration, q_e was equilibrium adsorption capacity, K_L was Langmuir constant). (a) Fitting of Ag^+ removal by 1T-MoS_2; (b) fitting of Ag^+ removal by 2H-MoS_2; (c) fitting of Pb^{2+} removal by 1T-MoS_2; (d) fitting of Pb^{2+} removal by 2H-MoS_2.

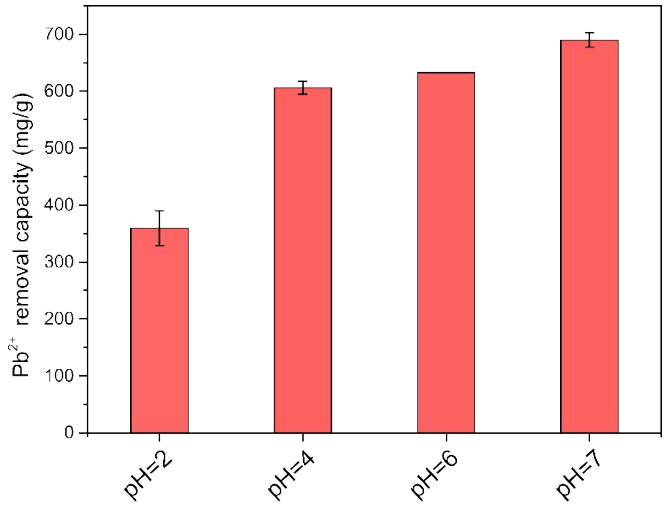

Figure S8. Pb^{2+} removals by 1T-MoS_2 nanosheets at different pH conditions.

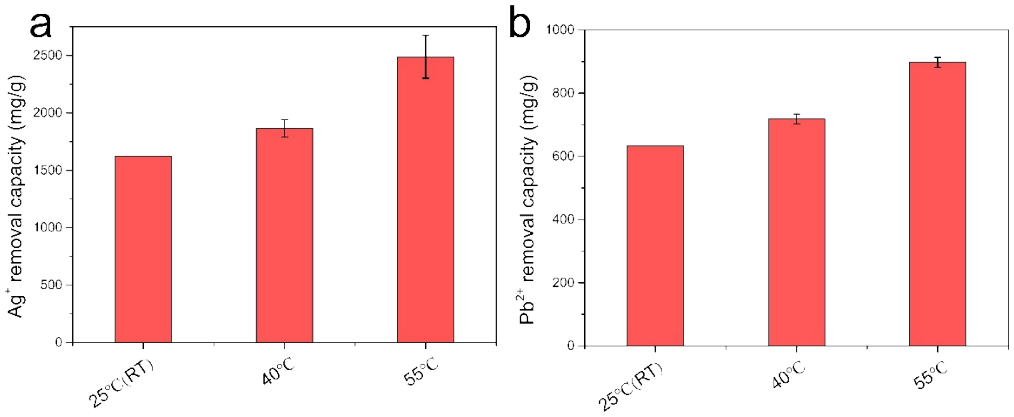

Figure S9. Ag^{+} and Pb^{2+} removals by 1T-MoS_2 nanosheets at different temperatures.

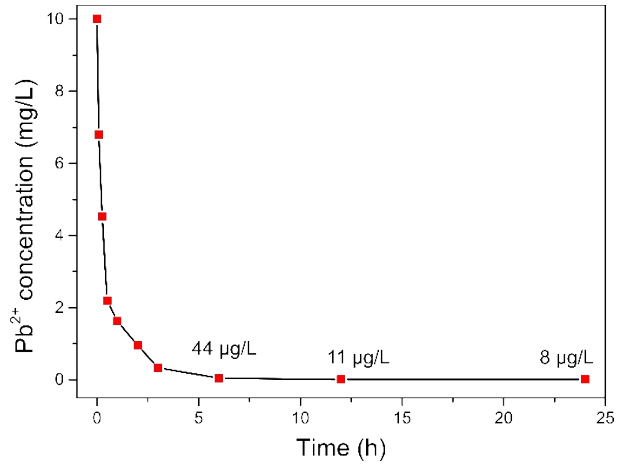

Figure S10. Removal kinetics of Pb^{2+} by 1T-MoS_2 within 1 d. The initial concentrations of Pb and MoS_2 were 10 and 100 mg/L, respectively.

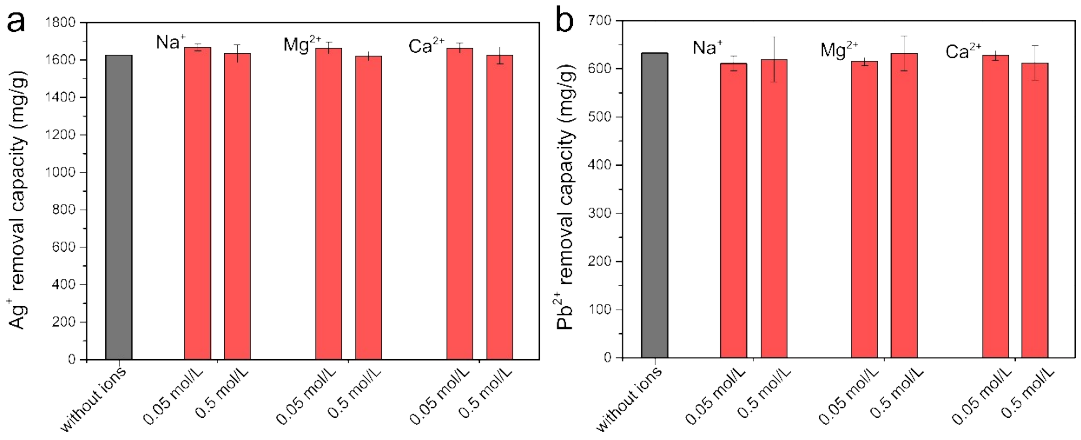

Figure S11 Removal capacity of (a) Ag^+ and (b) Pb^{2+} by 1T-MoS_2 (50 mg/L) in the absence and presence of common cations (Na^+, Mg^{2+}, Ca^{2+}) in different concentrations at pH 6. The initial concentration of Ag^+ or $Pb^{2+}$is 150 mg/L.

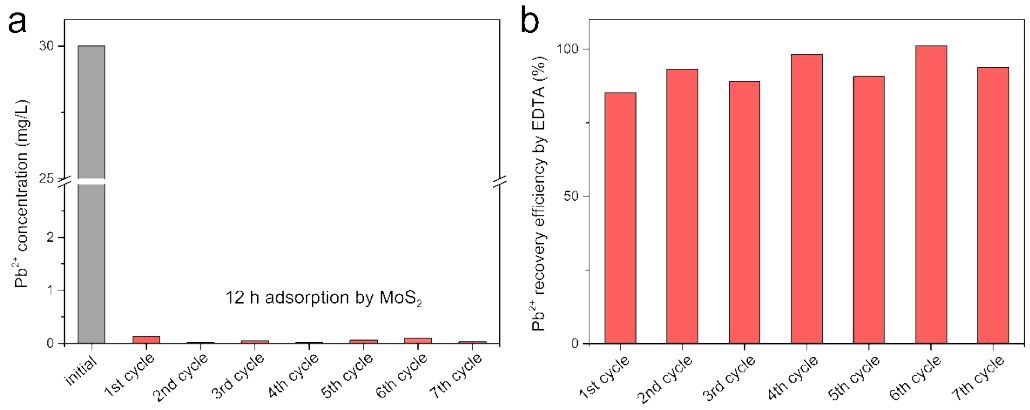

Figure S12. (a) Pb removals by stacked MoS_2 and (b) EDTA recovery efficiency in 7 consecutive tests.

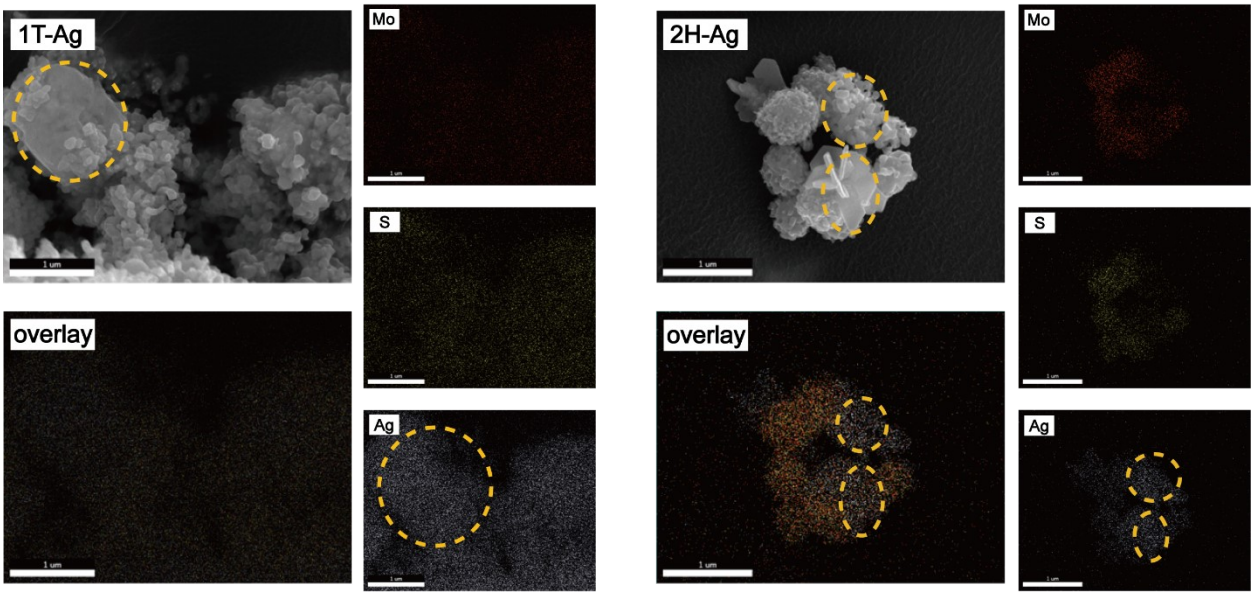

Figure S13. SEM images and EDS mapping of 1T-MoS_2-Ag^+ and 2H-MoS_2-Ag^+. The regions highlighted with orange dash line represent the presence of metallic Ag.

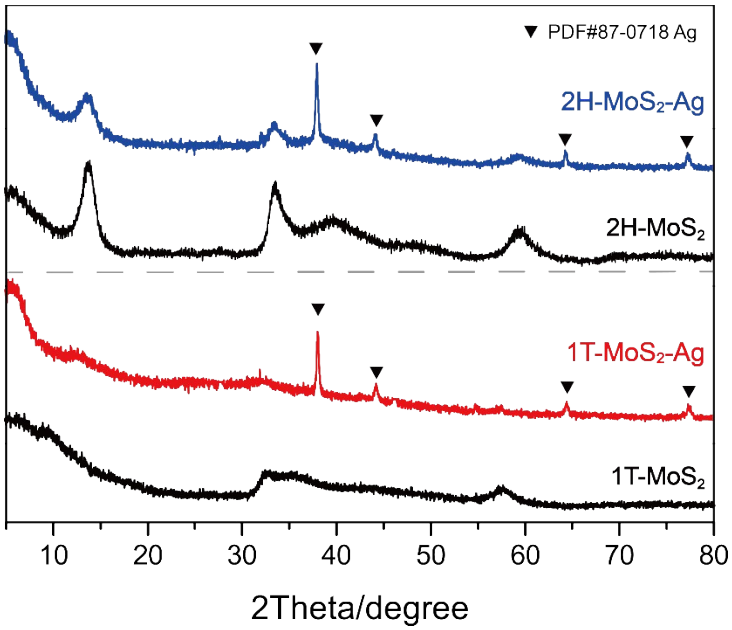

Figure S14. XRD patterns of 1T- and 2H-MoS_2 before and after Ag^+ removal.

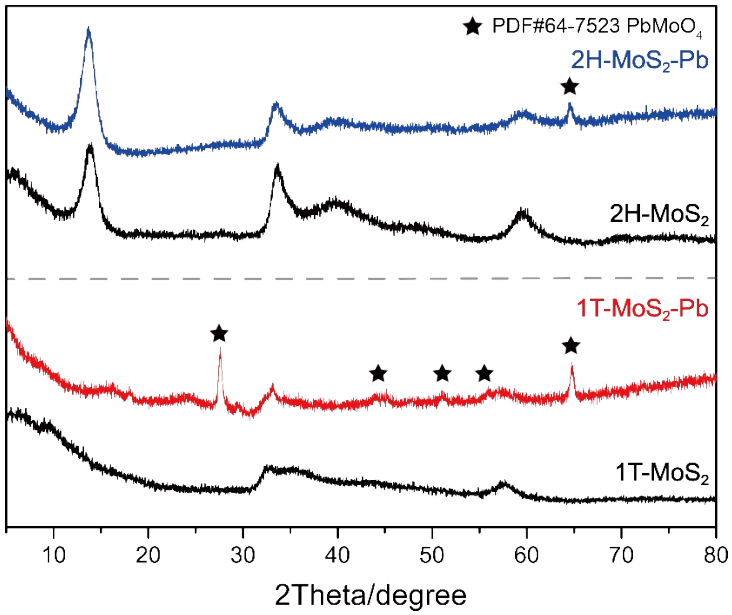

Figure S15. XRD patterns of 1T- and 2H-MoS_2 before and after Pb^{2+} removal.

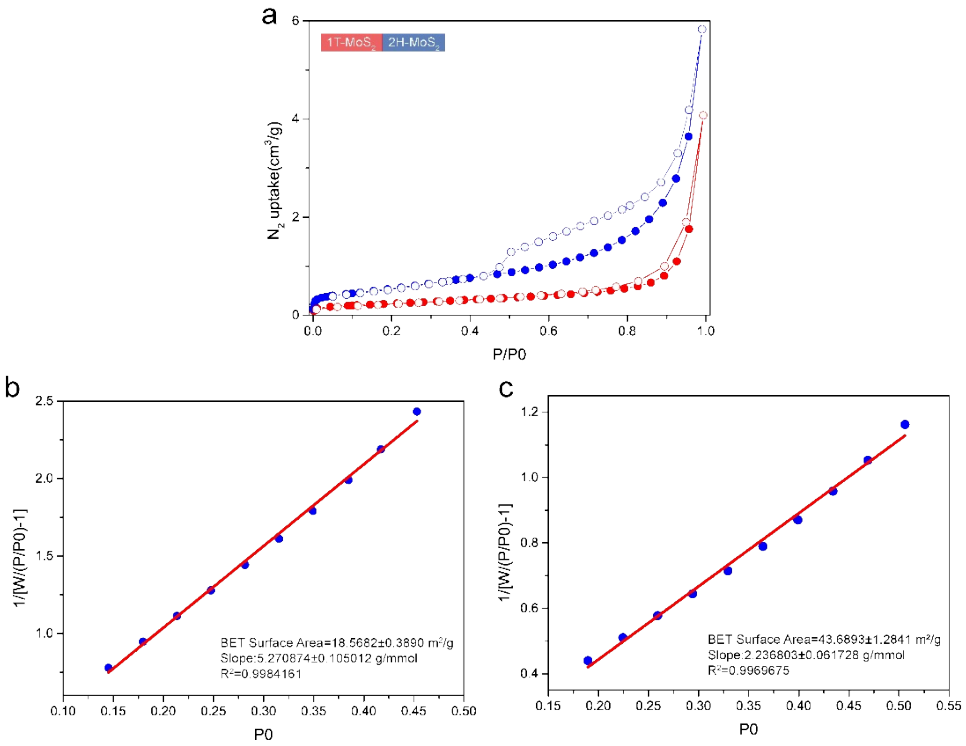

Figure S16. N_2 adsorption isotherm of 1T- and 2H-MoS_2 (a). BET surface area of 1T-MoS_2 (b). BET surface area of 2H-MoS_2 (c).

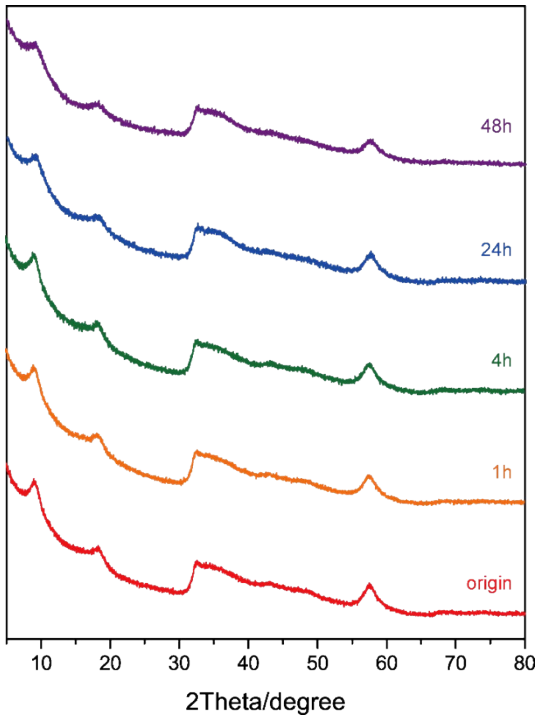

Figure S17. XRD patterns of as-synthesized 1T-MoS_2 sample dried in air from 1h to 48h.

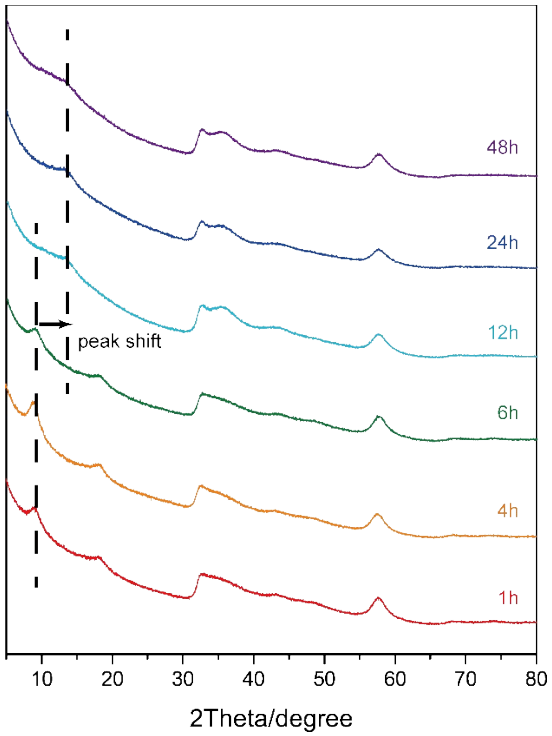

Figure S18. XRD pattern of as-synthesized 1T-MoS_2 sample dried in N_2 from 1h to 48h.

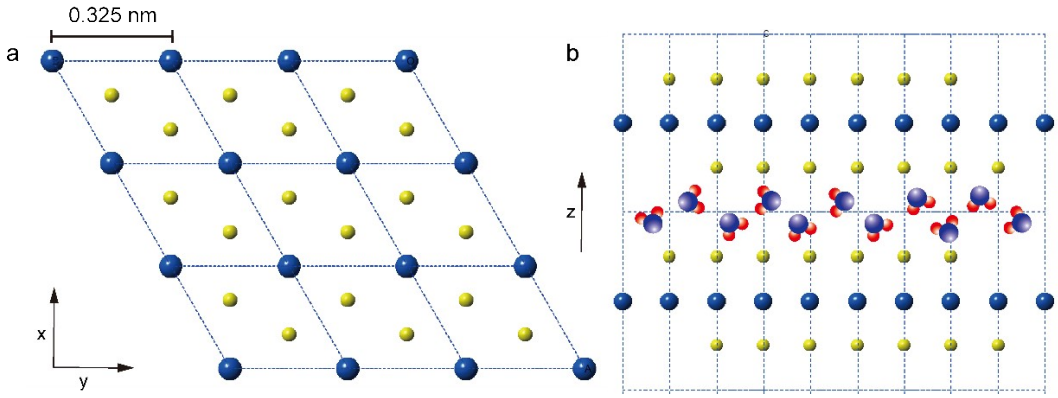

Figure S19. Crystal structure of 1T-MoS_2 in (a) the x-y plane and (b) the z direction (Yellow circles represent Mo atoms, blue circles represent S atoms). For as-synthesized 1T-MoS_2, an ~8 % weight loss was detected in the heating process at ~ 100℃. The lattice parameters of 1T-MoS_2 are a=b=3.25Å, c=6.14 Å, α=β=90°, γ=120°. The area of the 9-lattice crystal plane is 9.506×10^{-19} m^2. There are 16 molecules of MoS_2 in a 9-lattice unit cell, and 8 % of the total mass is accounted for by about 11.4 water molecules. The volume of a single water molecule is 3×10^{-29} m^3, so the volume of 11.4 water molecules is 3.42×10^{-28} m^3. If they are uniformly distributed throughout the crystal plane, the interlayer will increase by $\frac{3.42 \times 10^{-28}}{9.506 \times 10^{-19}}$=0.36 nm.

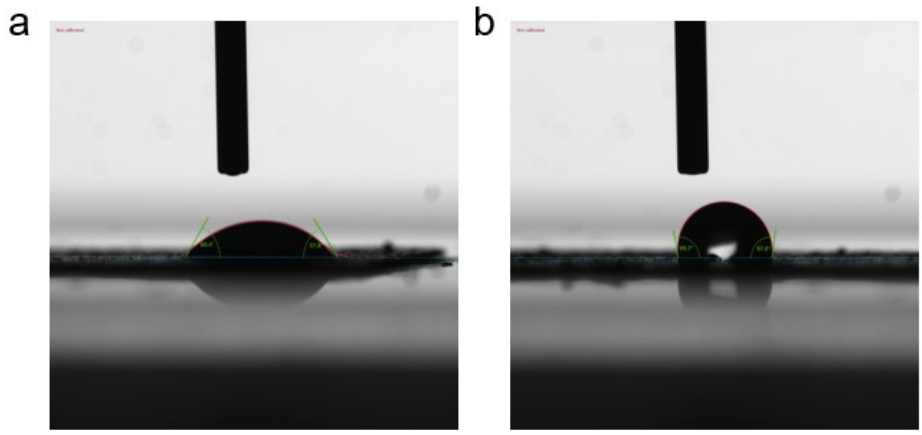

Figure S20. Contact angle testing of 1T-MoS_2 (a), 2H-MoS_2 (b).

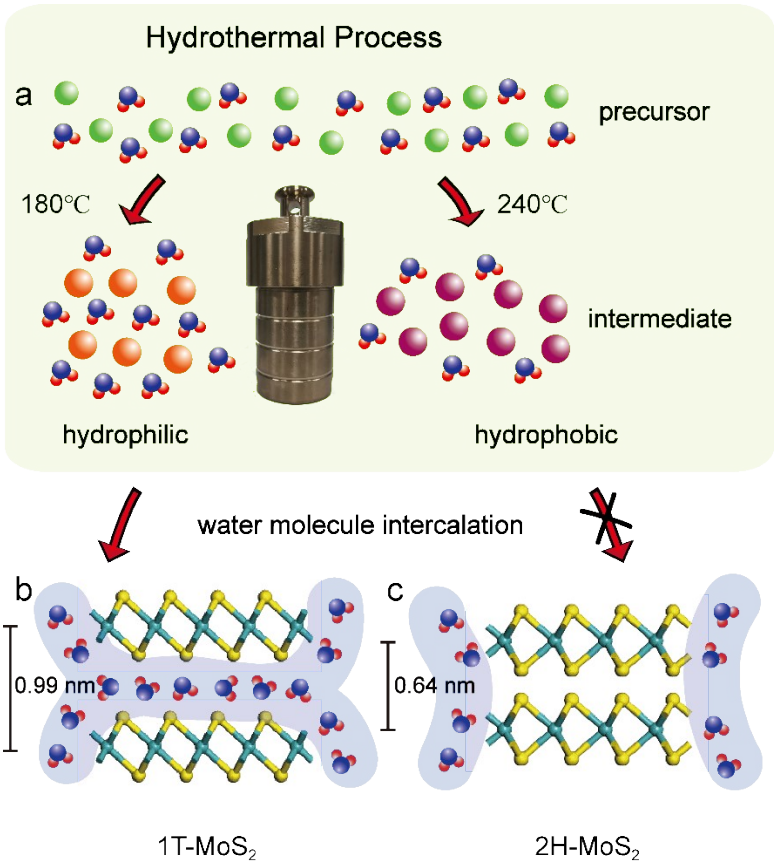

Figure S21. The schematic illustration of the formation process of spacing-varied nanochannels in 1T- and 2H-MoS_2 samples.

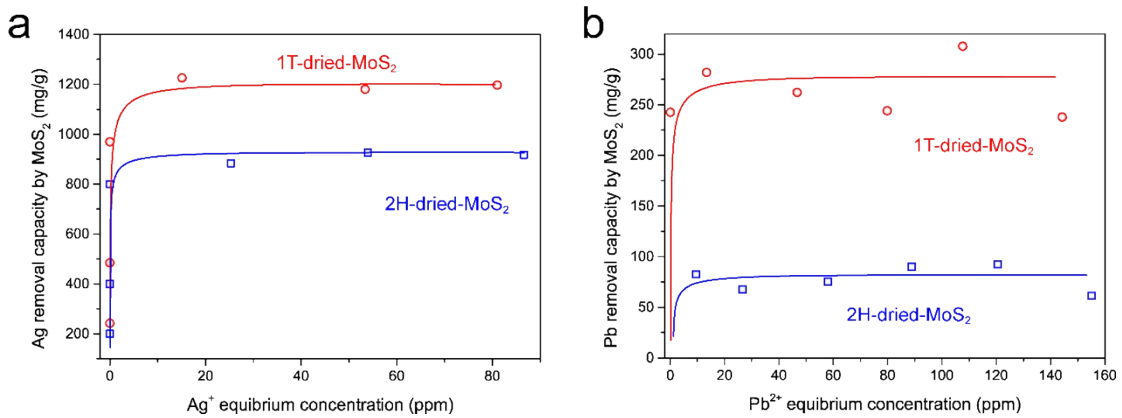

Figure S22. Removal capacity of Ag^{+} by dried 1T, 2H-MoS_2 (a) and Pb^{2+} by dried 1T-, 2H-MoS_2 (b). The initial concentrations of Ag^{+}, Pb^{2+} were 160 mg/L, and 1T-, 2H-MoS_2 concentration were 66 mg/L, 80 mg/L, respectively.

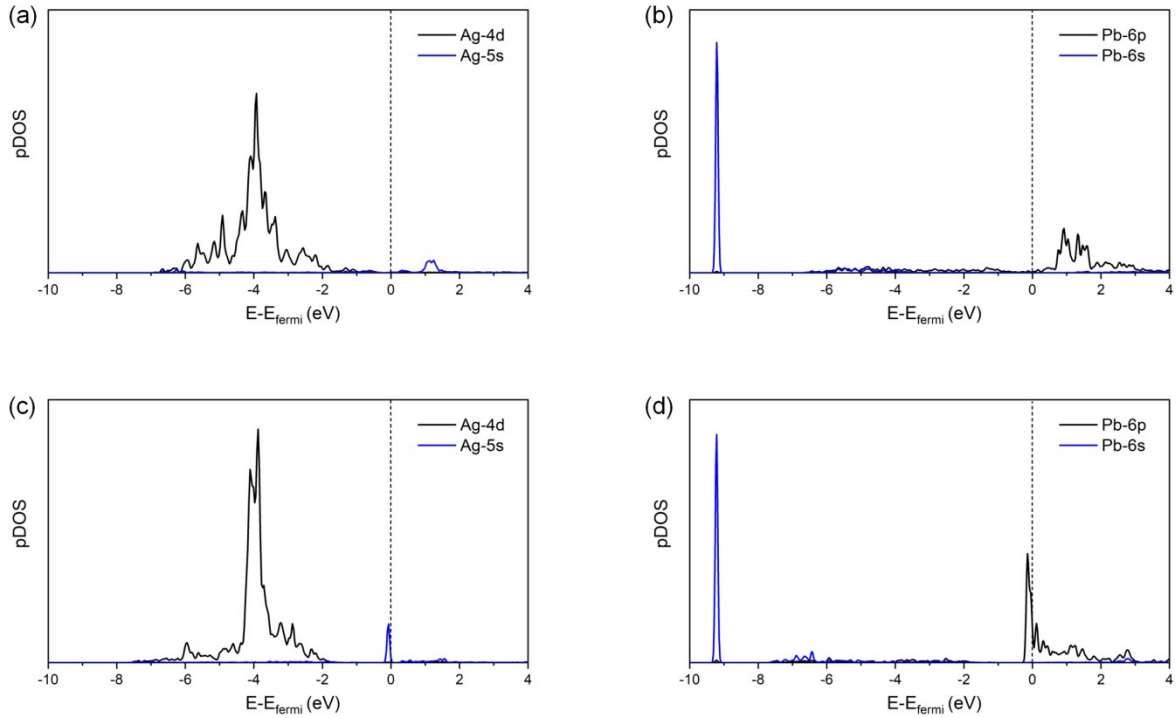

Figure S23. The projected density of states (pDOS). 4d, 5s orbitals of adsorbed Ag species and the 3p orbital of S on (a) 1T-MoS_2 and (c) 2H-MoS_2. 6p, 6s orbitals of adsorbed Pb species and 3p orbital of S on (b) 1T-MoS_2 and (d) 2H-MoS_2.

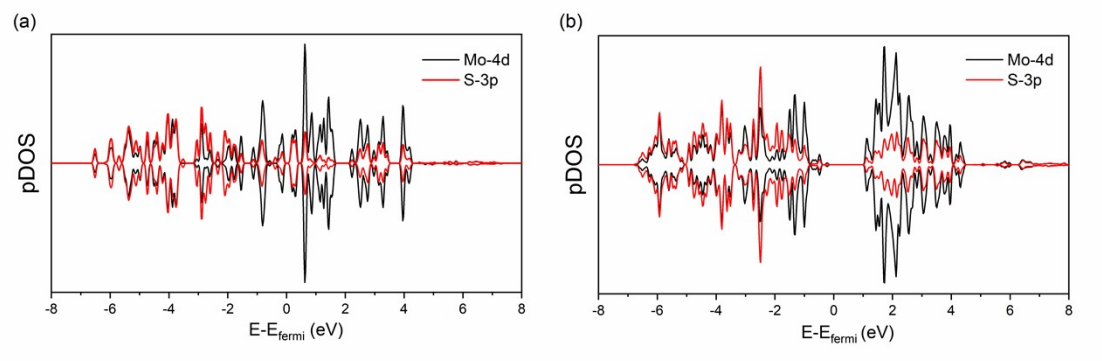

Figure S24. The projected density of states (pDOS) analysis for (a) 1T MoS_2 and (2) 2H-MoS_2. The band gap of 1T-MoS_2 is smaller than that of 2H-MoS_2, indicating that the 1T-MoS_2 is metallic, while the 2H phase of MoS_2 is semiconducting.

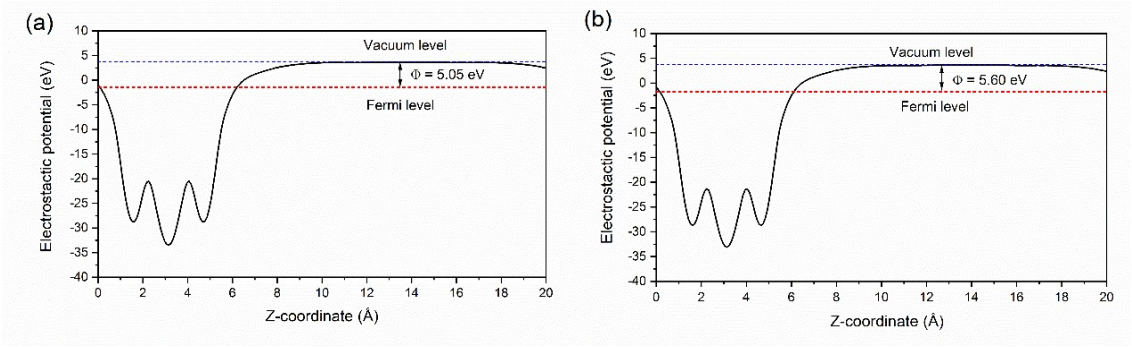

Figure S25. The work-functions (Φ) of (a) 1T-MoS_2 and (b) 2H-MoS_2.

Reference

1. Zhang, H.; Gu, L.; Zhang, L.; Zheng, S.; Wan, H.; Sun, J.; Zhu, D.; Xu, Z., Removal of aqueous Pb(II) by adsorption on Al2O3-pillared layered MnO2. *Appl. Surf. Sci.* **2017,** *406*, 330-338.

2. Liu, X.; Lai, D.; Wang, Y., Performance of Pb(II) removal by an activated carbon supported nanoscale zero-valent iron composite at ultralow iron content. *J. Hazard. Mater.* **2019,** *361*, 37-48.

3. Tan, Y.; Chen, M.; Hao, Y., High efficient removal of Pb (II) by amino-functionalized Fe3O4 magnetic nano-particles. *Chem. Eng. J.* **2012,** *191*, 104-111.

4. Karthik, R.; Meenakshi, S., Removal of Pb(II) and Cd(II) ions from aqueous solution using polyaniline grafted chitosan. *Chem. Eng. J.* **2015,** *263*, 168-177.

5. Ren, X.; Shao, D.; Yang, S.; Hu, J.; Sheng, G.; Tan, X.; Wang, X., Comparative study of Pb(II) sorption on XC-72 carbon and multi-walled carbon nanotubes from aqueous solutions. *Chem. Eng. J.* **2011,** *170*, (1), 170-177.

6. Abdollahi, N.; Akbar Razavi, S. A.; Morsali, A.; Hu, M.-L., High capacity Hg(II) and Pb(II) removal using MOF-based nanocomposite: Cooperative effects of pore functionalization and surface-charge modulation. *J. Hazard. Mater.* **2020,** *387*, 121667.

7. Bao, S.; Yang, W.; Wang, Y.; Yu, Y.; Sun, Y., One-pot synthesis of magnetic graphene oxide composites as an efficient and recoverable adsorbent for Cd(II) and Pb(II) removal from aqueous solution. *J. Hazard. Mater.* **2020,** *381*, 120914.

8. Fan, J.; Cai, C.; Chi, H.; Reid, B. J.; Coulon, F.; Zhang, Y.; Hou, Y., Remediation of cadmium and lead polluted soil using thiol-modified biochar. *J. Hazard. Mater.* **2020,** *388*, 122037.

9. Wang, Z.; Tu, Q.; Sim, A.; Yu, J.; Duan, Y.; Poon, S.; Liu, B.; Han, Q.; Urban, J. J.; Sedlak, D.; Mi, B., Superselective Removal of Lead from Water by Two-Dimensional MoS2 Nanosheets and Layer-Stacked Membranes. *Environ. Sci. Technol.* **2020**.

10. Luo, J.; Fu, K.; Sun, M.; Yin, K.; Wang, D.; Liu, X.; Crittenden, J. C., Phase-Mediated Heavy Metal Adsorption from Aqueous Solutions Using Two-Dimensional Layered MoS2. *ACS Appl. Mater. Interfaces* **2019,** *11*, (42), 38789-38797.

11. Jayadharan Salini, A. N.; Ramachandran, A.; Sadasivakurup, S.; Yesodha, S. K., Versatile MoS_2 hollow nanoroses for a quick-witted removal of Hg (II), Pb (II) and Ag (I) from water and the mechanism: Affinity or Electrochemistry? *Appl. Mater. Today.* **2020,** *20*, 100642.

12. Liu, Y.; Ma, C.; Zhang, X.; Ngo, H. H.; Guo, W.; Zhang, M.; Zhang, D., Role of structural characteristics of MoS2 nanosheets on Pb2 + removal in aqueous solution. *Environ. Technol. Innovation* **2021,** *22*, 101385.

13. Kumar, N.; Fosso-Kankeu, E.; Ray, S. S., Achieving Controllable MoS2 Nanostructures with Increased Interlayer Spacing for Efficient Removal of Pb(II) from Aquatic Systems. *ACS Appl. Mater. Interfaces* **2019,** *11*, (21), 19141-19155.

14. Liu, C.; Zeng, S.; Yang, B.; Jia, F.; Song, S., Simultaneous removal of Hg^{2+}, Pb^{2+} and Cd^{2+} from aqueous solutions on multifunctional MoS_2. *J. Mol. Liq.* **2019,** *296*, 111987.

15. Wang, J.; Zhang, W.; Yue, X.; Yang, Q.; Liu, F.; Wang, Y.; Zhang, D.; Li, Z.; Wang, J., One-pot synthesis of multifunctional magnetic ferrite–MoS2–carbon dot nanohybrid adsorbent for efficient Pb(ii) removal. *Journal of Materials Chemistry A* **2016,** *4*, (10), 3893-3900.

16. Pytlakowska, K.; Kocot, K.; Hachuła, B.; Pilch, M.; Wrzalik, R.; Zubko, M., Determination of heavy metal ions by energy dispersive X-ray fluorescence spectrometry using

reduced graphene oxide decorated with molybdenum disulfide as solid adsorbent. *Spectrochim. Acta, Part B* **2020,** *167*, 105846.

17. Zhu, H.; Tan, X.; Tan, L.; Chen, C.; Alharbi, N. S.; Hayat, T.; Fang, M.; Wang, X., Biochar Derived from Sawdust Embedded with Molybdenum Disulfide for Highly Selective Removal of Pb2+. *ACS Appl. Nano Mater.* **2018,** *1*, (6), 2689-2698.

18. Zolgharnein, J.; Rastgordani, M., Multivariate optimization and characterization of simultaneous removal of binary mixture of Cu(II) and Pb(II) using Fe3O4@MoS2 nanoparticles. *J. Chemom.* **2018,** *32*, (9), e3043.

19. Wang, Q.; Peng, L.; Gong, Y.; Jia, F.; Song, S.; Li, Y., Mussel-inspired Fe3O4@Polydopamine(PDA)-MoS2 core–shell nanosphere as a promising adsorbent for removal of Pb2+ from water. *J. Mol. Liq.* **2019,** *282*, 598-605.

20. Pandey, S.; Fosso-Kankeu, E.; Spiro, M. J.; Waanders, F.; Kumar, N.; Ray, S. S.; Kim, J.; Kang, M., Equilibrium, kinetic, and thermodynamic studies of lead ion adsorption from mine wastewater onto MoS2-clinoptilolite composite. *Mater. Today Chem.* **2020,** *18*, 100376.

21. Wang, Z.; Zhang, J.; Wen, T.; Liu, X.; Wang, Y.; Yang, H.; Sun, J.; Feng, J.; Dong, S.; Sun, J., Highly effective remediation of Pb(II) and Hg(II) contaminated wastewater and soil by flower-like magnetic MoS2 nanohybrid. *Science of The Total Environment* **2020,** *699*, 134341.